Synthesis and Microwave Dielectric Properties of Tin-Doped Barium Titanate Ceramics

Muhammad Anas[1], Asad Ali[1*], Muhammad Hasnain Jameel[2], Mursel Alper[3], Maytham Qabel Hamzah[4,5], Shakirullah[1] and Shayan Ali[1]

[1]*Department of Physics, Govt Post Graduate College Nowshera, Khyber Pakhtunkwa, Pakistan.*
[2]*Institute of Modern Physics Northwest University Xi'an China.*
[3]*Physics Department, Science & Literature Faculty, Bursa Uludağ University, Görükle, 16059, Bursa, Turkey.*
[4]*Department of Physics and Chemistry, University Tun Hussein Onn Malaysia, 83000 Malaysia.*
[5]*General Directorate of Education in Al-Muthanna Governorate, Ministry of Education, Republic of Iraq.*

Authors' contributions

This work was carried out in collaboration among all authors. Authors AA, MA, SA and Shakirullah designed the study, performed the statistical analysis, wrote the protocol and wrote the first draft of the manuscript. Authors MHJ and MQH managed the analyses of the study. Author MA managed the literature searches. All authors read and approved the final manuscript.

Original Research Article	

ABSTRACT

Tin- Doped Barium Titanate Ceramics is a multiferroic substance that displays an important role in electronic devices. Manufacturing of energy storage devices with good efficiency and fewer losses has been a distinct topic. In the current study, Solid solution of Tin-doped Barium Titanate substitution with (x = 0, 0.5) synthesized through mixed oxide conventional technique and calcined at 800°C temperature for 3h with heating/cooling at rate 5°C/min. The structural, optical, and microwave dielectric properties were studied by SEM (Scanning electron microscopy) X-ray diffraction, photoluminescence spectroscopy, Fourier transform infrared, and vector network analyzer, respectively. X-ray diffraction (XRD) study shows that the crystal phase structure, hkl planes, the lattice constant, average crystallite size, and volume unit cell of Tin- Doped Barium Titanate. XRD shows grain size reduces with increasing Sn^{4+} content. An intense and broadband

spectrum was observed at around the red color emission region. Optimum dielectric properties i.e. high dielectric constant (ϵ_r = 40.5), high quality factor (Q = 13,106) and low dielectric loss (0.00013) at 0.15 GHz frequency have been observed. The SEM image shows an inhibited grain growth with an increase of Sn^{4+} content. The results demonstrate that it is the possibility of tuning Ba(Ti1-xSnx)O3 optic and microwave dielectric properties by doping different concentrations of Tin nanoparticles.

1. INTRODUCTION

Tin- Doped Barium Titanate Ceramics materials are presenting a major role in the electronic devices with the best stability and high ferroelectric transition temperatures. Amongst the multiferroic ceramics or materials that have been rigorously investigating, $[Ba(Ti_{1-x}Sn_x)_4O_9]$ is considered as potential material for unique applications, Fast electrical polarization control by a magnetic field or by magnetization. Barium titanate ceramics material has wide applications in microwave (MW) telecommunication technologies, e.g., global positioning system (GPS), satellite broadcasting, cellular phones, and air traffic control system [1-3]. The major objective of recent research in this field is to design new ceramics material or to modify the microwave dielectric properties, i.e., such as near to zero temperature coefficients of resonant frequency (τ_f), high dielectric constant (ϵ_r) and low dielectric loss (tanδ) of already known ceramic materials. Masse et al. reported low dielectric loss barium titanate (BT) dielectric resonator (DR) for the first time in the early 1970s [4]. BT plays a vital role in the breakthrough in MW-wireless communication or dielectric ceramics technology. BT samples had been fabricated through a conventional mixed-oxide route using horizontal ball milling of the mixtures of reactants TiO_2 and $BaCO_3$ for 24h [5,6]. Cernea et al. obtained BT samples from the wet chemical method and recorded dielectric constant (37), dielectric loss (0.0017), and temperature coefficient of resonant frequency (11ppm/°C [7]. The microwave dielectric, optical and structural characteristics of BT specimen with several different properties have also been analyzed in the microwave range [8-11]. Many studies have been carried out on the substitution in the B site. By doping with different ions [Sn^{4+}] and [Ti^{4+}], the bandgap of $[Ba(Ti_{1-x}Sn_x)_4O_9]$ can be reduced. Doping of [Sn^{4+}] and [Ti^{4+}] ferrite with any element may influence its electrical, optical, magnetic, magneto-electric, and structural properties. The influence of the substitution of Sn^{4+} ions for Ti^{4+} ions plays an important role in the enhancement of microwave properties [12-14]. The Sn^{4+} element has received considerable attention because of its extraordinary role in $[Ba(Ti_{1-x}Sn_x)_4O_9]$ thin films. Veenhuis et al. reported that BT-based samples showed favorable applications in the field of electronic or optical storage devices, advanced laser technologies, etc. [15].

The major aim of the present work is to synthesize and characterize low loss dielectrics with improved dielectric and optical properties through analyzing the effects of doping Sn^{4+} for Ti^{4+} in $[Ba(Ti_{1-x}Sn_x)_4O_9]$ (with x = 0.0, 0.5) composition.

2. EXPERIMENTAL PROCEDURES

The solid solution of barium titanate $Ba(Ti_{1-x}Sn_x)O_3$ (x = 0, 0.5) ceramics composition was obtained through conventional mixed oxides route. Analytical grades of powders of high pure oxide were used in the beginning as raw materials such as BaCO3 (Merck), TiO_2, and SnO_2 (Strems, Additives, U.S.A). (99.9 percent). Stoichiometric oxides concentration was weighed bestowing to composition and for 24h ball-mixed in distilled water (wetting media). The mixture was dried at 90°C in an oven, and the dried mixture was calcined at 800°C for high purity for 3h through alumina crucible in the air at five °C/min cooling/heating rate in a conventional furnace to yield $Ba(Ti_{1-x}Sn_x)O_3$ (x = 0, 0.5) powders. The calcined mixtures were grinded manually with a mortal and pistol for 12h to avoid agglomeration. The fine powders were filled into 10mm pellets in diameter and the thickness of pellets 5mm under a pressure of 7 ton/in^2 using a manual pellet press (CARVER, USA). At a temperature of 1320°C, samples of pellets were sintered in the air for 2 hours with a heated/cooling speed of 5°C/min. In the calcined ceramics samples, crystalline phases were analyzed with radiation 40mA and 40kV by using X-rays diffractometer (XRD) (JDX-3532, JEOL, Japan) with Cu Kα (λ = 0.15406 nm) functioned at in an extensive range of Braggs angles 2θ

$(10° < 2\theta < 90°)$ at a scanning rate of 2°/min. An electronic densimeter (MD-3005) was used to measure the experimental densities of the samples. Scan electron microscopy (SEM, JEOL 7600F) operated at 15 k V was used for the moral studies of the sample sintered. The Fourier transformation infrared spectroscopy (FTIR) absorption spectrum was recorded on a Perkin-Elmer GX FTIR system was used to obtain 10 cm^{-1} resolution spectrum in the range 400 to 4000 cm^{-1} region. The photoluminescence spectroscopy (PL) spectrum was recorded on a Jobin Yvon-Horiba Triax 190 spectrometer with 0.30 nm resolution spectrum. The dielectric properties of sintered ceramic samples were measured by using a vector network analyzer (ZVB20, Rohde & Schwarz, Germany).

3. RESULTS AND DISCUSSION

3.1 Structural Analysis

Fig. 1 shows the X-ray diffraction patterns of the Sn-doped in barium titanate ($BaTiO_3$) sintered ceramic at 920 °C for 3hrs in air. The XRD patterns show that they are all single-phase tetragonal structures (which can be indexed as $BaTiO_3$) and matched with JCPDS card # 05-0626 with space group Amm2 [16]. These results demonstrated that with the replacement of Ti^{4+} by Sn^{4+}, $Ba(Ti_{1-x}Sn_x)O_3$ at (x = 0.0, 0.5) composition would form a solid solution. XRD results show that the positions of the diffraction peaks of the ceramics shift slightly to lower angle with increasing Sn^{4+} content in the region of 2θ from $38°$ to $48°$. The greater Sn^{4+} (0.069nm) ionic radius, relative to Ti^{4+} (0.060nm), contributes to a small improvement in crystal cell volumes, and hence a shift of diffraction peaks towards lower angles. The crystallite size of each major peak can be measured through the Debye Scherer's formula [17] and observed approximately 21.0 nm average crystallite size, as shown in Table 1.

$$D = \frac{0.9\lambda}{\beta Cos\theta} \qquad \text{Eq. (1)}$$

Where 'D' is the size of crystallite, the wavelength (λ) of Cu Kα radiation, 'θ' is the brags angle and 'β' is the full-width at half-maximum (FWHM). The average crystallite size of BT sample was reported to be 15.0 nm [18].

3.2 Structural Analysis

Each figure should have a caption. The caption should be concise and typed separately, not on the figure area. Figures should be self-explanatory. Information presented in the figure should not be repeated in the Table. All symbols and abbreviations used in the illustrations should be defined clearly. Figure legends should be given below the figures. A sample figure is given in Fig. 1.

The secondary electron images (SEIs) with different resolutions, from thermally etched and gold-coated $Ba(Ti_{1-x}Sn_x)O_3$ ($X = 0.0, 0.5$) ceramic samples sintered at 920°C for 3 hrs is shown in Fig 2. Both these are samples dense and have distinct microstructural properties with the existence of cavities. The presence of cavities in the SEM results shows that the samples in the pellets have a small amount of porosity. The grain size and grain boundaries can be seen very obviously in a non-agglomerated section, and the particle size reduces by increasing Sn4+ substitution. Porosity can be decreased by increasing the relative density of the sample [19]. We have calculated the porosity of the samples using equation (2) and observed a small value of porosity at x = 0.5 Sn4+ content, as shown in Table 2.

$$\text{Porosity} = \left(\frac{\rho_{th} - \rho_{ex}}{\rho_{th}}\right) \times 100\% \qquad \text{Eq. (2)}$$

Densification is further induced by Sn4+ content (x = 0.5), which tends to reduce particle growth [20]. In SEM microstructures images showed in Figs. 3-6, this improvement in density also indicates decreased porosity.

3.3 Optical Properties

Fig. 3 shows the FTIR pattern of fabricated compound $Ba(Ti_{1-x}Sn_x)O_3$ (with x = 0.0, 0.5) ceramic material. A strong absorption peak can be seen near 466, 1437, and $2926cm^{-1}$. FTIR results show that [21], these peaks characterize the vibration of Ti-O octahedron. The absorption peak of pure $BaTO_3$ is 855 and 2853 cm^{-1}. It can be shifted by subsisting of Tin and (Sn) additives to 861 and 2859 cm^{-1}, respectively. The only one O-vacancy can be formed by replacing Ba^{2+}, and three O-vacancies are produced by replacing Ti^{4+} by means of respective additives [22]. In this way, Ti-O octahedrons are damaged or distorted easily. Several vibrations modes were observed in the FTIR spectrum. Therefore, the comparative study of the FTIR spectra further supports the improvement of the redispersibility of the polycrystalline barium tetra titanate dielectric material.
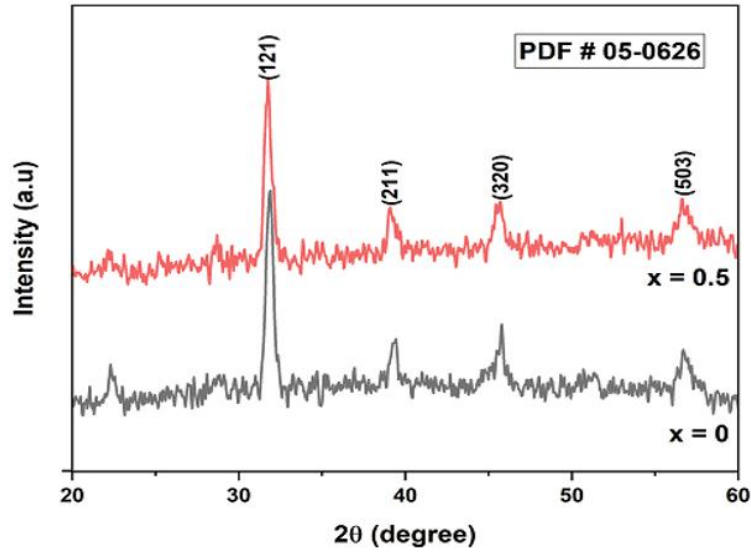
Fig. 1. XRD pattern of Ba(Ti$_{1-x}$Sn$_x$)O$_3$ (with x = 0.0, 0.5) sintered ceramic at 920°C

Table 1. Crystallite size of each plane of barium titanate ceramics

Planes	Brags angle (2θ) (degree)	Brags angle (θ) (degree)	FWHM (β) (degree)	FWHM (β) (radian)	Crystallite size (D) (nm)
(121)	31.85	15.92	0.551	0.0096	15.0
(211)	39.1	19.55	0.375	0.0065	21.71
(320)	45.65	22.82	0.406	0.0071	19.88
(503)	56.6	28.3	0.627	0.011	14.03
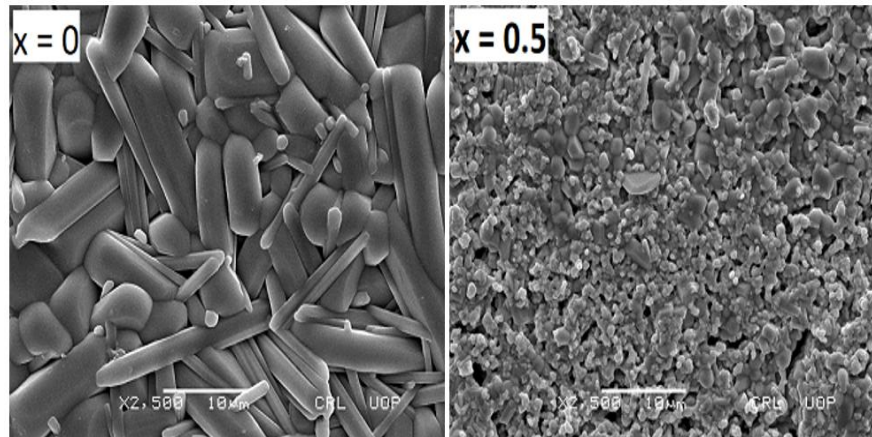
Fig. 2. SEM Micrograph for x = 0 and x = 0.5 in the system of Ba(Ti1-xSnx)O3 sintered ceramic at 920°C for 3 h

Table 2. Physical properties of [Ba(Ti$_{1-x}$Sn$_x$)$_4$O$_9$] (with x = 0.0, 0.5) ceramics

Sample	Theoretical density (ρth), (gm/cm3)	Experimental density (ρex), (gm/cm3)	Relative density (ρre), (%)	Porosity (%)
(320)	45.65	22.82	0.406	0.0071
(503)	56.6	28.3	0.627	0.011
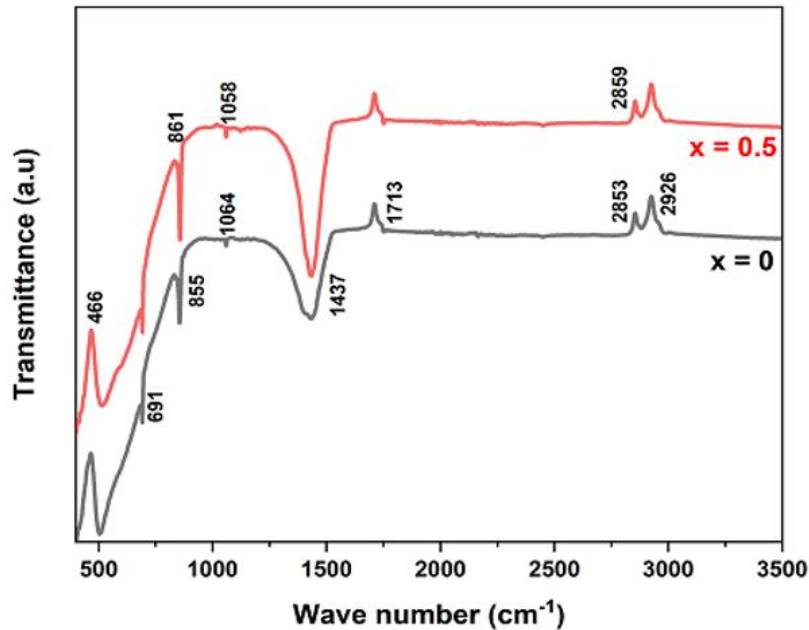
Fig. 3. FTIR spectra of Ba(Ti$_{1-x}$Sn$_x$)O$_3$ (with x = 0.0, 0.5) sintered ceramic at 920°C for 3 h

Photoluminescence (PL) spectra of $Ba(Ti_{1-x}Sn_x)O_3$ with substituting x = 0, 0.5 calcined ceramic at 920°C for three h excited with 488nm laser beam source at normal room temperature shown in Fig. 4. PL spectra of sample material have defected related deep level emission in the visible range of the optical spectrum. The emission in the visible region is recognized to the recombination of holes and electrons in the state of delocalization. This state of delocalization is because of the intrinsic morphological, structural defect interrelated to Ti^{4+} microcrystal symmetric in the microphase of BaTiO$_3$. The PL emission spectra of the sample is recorded red color (604.6 nm) with excitation energy (2.05 eV) at x = 0 content and (605.8nm) with excitation energy (2.04 eV) at x = 0.5 content respectively. This red color represented the electronic transition produced by various degrees of morphological order-disorder in the sample [23]. PL is a typical multi-photon method that is an emission occurred in optical energy gape by many vibrational states within it. This can be confirmed that PL is directly related to the existing localized state within the bandgap, which affected the structural order-disorder directly. Therefore, the structural order increases with increasing the band gape energy [24]. It has been analyzed that a wide emission band is found at ~604.6nm and has excitation energy

(~2.05 eV) smaller than the bandgap energy of extremely ordered barium tetra titanate located at ~558 nm (~2.23 eV), which is due to the oxygen vacancy [25]. In this PL

characteristic, the oxygen vacancy act is a red color emitted source.

3.4 Microwave Dielectric Properties

The dielectric loss (tan δ) and dielectric constant (ϵ$_r$) in the frequency range of 100MHz–800MHz of $Ba(Ti_{1-x}Sn_x)O_3$ with x = 0.0, 0.5 sintered ceramic at normal temperature is shown in Fig. 5. It can be observed that dielectric constant value at x = 0.5 content, which is higher than that of x = 0 content. The relative permittivity of both samples is almost remaining constant with increasing frequency. The increase in the relative permittivity due to Sn doping may be the result of decreasing the particle size and increasing the densification of the specimen. The dielectric loss of the sample increases exponentially with increasing frequency. In the region of lower frequency, a decrease in the value of the dielectric loss was analyzed, which is because of the dominance of space charge polarization and orientational charge polarization of the sample [26-28]. We have observed optimum dielectric properties at x = 0.5 content.
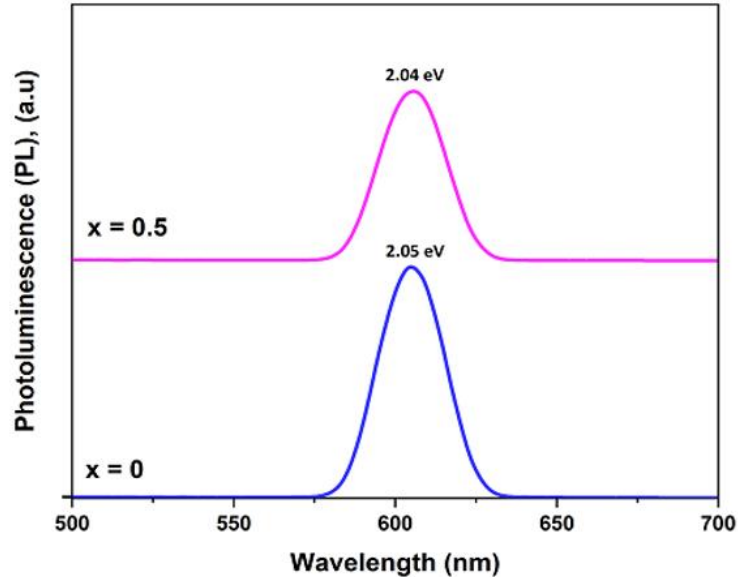
Fig. 4. PL spectra of $Ba(Ti_{1-x}Sn_x)O_3$ substituting with x = 0.0, 0.5 sintered ceramic at 920°C for 3h
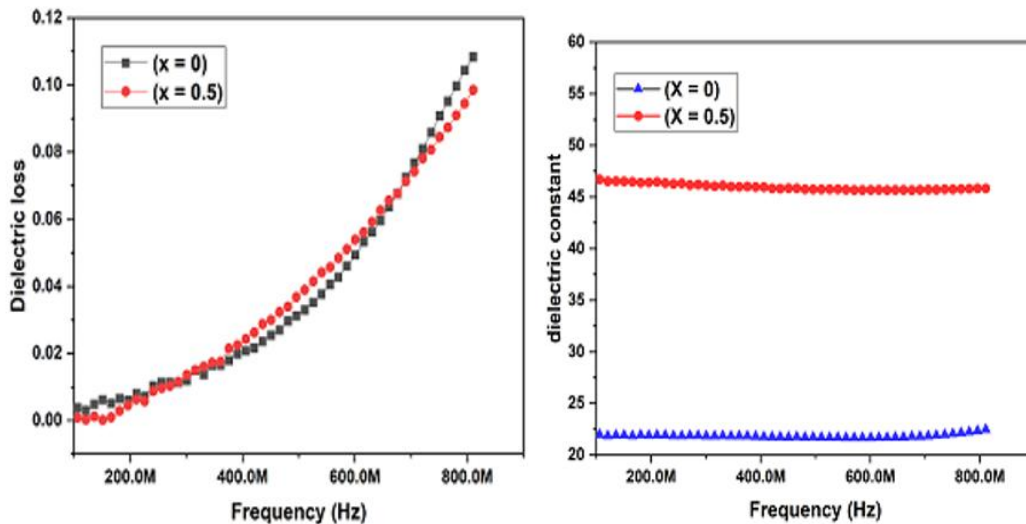
Fig. 5. Variation of dielectric loss and dielectric constant vs. frequencies of $Ba(Ti_{1-x}Sn_x)O_3$ with substituted at x = 0.0, 0.5) sintered ceramic at 920 °C for 3h

4. CONCLUSION

Lead free Sn^{4+} doped barium titanate of $Ba(Ti_{1-x}Sn_x)O_3$ (with x = 0.0, 0.5) were fabricated through conventional mixed oxide route. The XRD pattern revealed that the sample has a tetragonal structure. XRD shows grain size reduces with increasing Sn^{4+} content. An intense and broadband spectrum was observed at around the red color emission region. The SEM image shows an inhibited grain growth with an increase of Sn^{4+} content. An intense and broadband spectrum was observed at around the red color emission region. Optimum dielectric properties i.e. high dielectric constant (ϵ_r = 40.5), high quality factor (Q = 13,106) and low dielectric loss (0.00013) at 0.15 GHz frequency have been observed. The SEM image shows an inhibited grain growth with an increase of Sn^{4+} content. The results demonstrate that it is the possibility of tuning $Ba(Ti_{1-x}Sn_x)O_3$ optic and microwave dielectric properties by doping different concentrations of Tin nanoparticles.

ACKNOWLEDGEMENTS

COMPETING INTERESTS

Authors have declared that no competing interests exist.

REFERENCES

1. Sebastian MT. in Dielectric materials for wireless communication, Elsevier B.V, Great Britain: 1st edition; 2008.
2. Hamzah MQ, Jabbar AH, Mezan SO, Tuama AN, Agam MA. Fabrications of PS/TiO2 nanocomposite for solar cells applications," in AIP Conference Proceedings; 2019.
   DOI: 10.1063/1.5124641
3. Yabagi JA, Kimpa MI, Muhammad BL, Hamzah MQ, Kadir HKA, Arif Agam M. The Effect of Silver Particles on the Synthesis and Characterization of Polystyrene/Silver (Ps/Ag) Nanocomposites for Carbonaceous Materials. Int. J. Nanoelectron. Mater. 2020;13(2):263–282.
4. Masse DJ, Pucel RA, Readey DW, Maguire EA, Hartwig CP. Proceedings of the IEEE. 1971;59(11):1628-1629.
5. Mhaisalkar SG, Lee WE, Readey DW. J. Am. Ceram. Soc. 1989;72(11):2154–2158.
6. Mhaisalkar SG, DW. Readey and S. A. Akbar. J. Am. Ceram. Soc. 1991;74(8): 1894–1898.
7. Cernea M, Chirtop E, Neacsu D et al. Journal of the American Ceramic Society. 2002;85(2):499–503.
8. Mhaisalkar SG, Readey DW, Akbar SA et al. J. Solid State Chem. 1991;95(2):275-284.
9. Nishigaki S, Yano S, Kato H et al. J. Am. Ceram. Soc. 1988;71(1):C-11-C17.
10. Ern V, Newnham RE. J. Am. Ceram. Soc. 1961;44(4):199-205.
11. Mhasalkar SG, Lee WE, DW Readey. J. Am. Ceram. Soc. 1989;72(1):2154-2160.
12. Mueller V, Beige H, Abicht HP. Appl. Phys. Lett. 2004;84:1341.
13. Lu SG, Xu ZK, Chen H. Appl. Phys. Lett. 2004;85:5319.
14. Shvartsman VV, Kleemann W, Dec J, Xu ZK, Lu SG. J. Appl. Phys. 2006;99:124111
15. Veenhuis H et al. J. Appl. Phys. 2002; 70(6):797-801.
16. Chen YB, Liu SS. Journal of Materials Science: Materials in Electronics. 2019;30: 5567–5572.
17. Patterson AL. Phys. Rev. 1939;56:978-986.
18. Tao J. et al. Mater. Res. Bull. 2008;43:639-645.
19. Mahajan S, et al. J. Bull. Mater. Sci. 2011;34 (7):1483–1489.
20. Naboulsia TA, Boulos M, Tenailleau C, Dufour P, Zakhour M, Sophie GF. Journal of Ceramic Processing Research. 2016;17(8):870-875.
21. Perry CH, Khanna BN. Phys. Rev. 1957; 105:A408.
22. Sun D. et al. J. Ferroelectrics. 2007;355: 145–148.
23. Longo VM, Cavalcante LS, Figueiredo AT. et al. Appl. Phys. Lett. 2007;90:906-911.
24. Leite ER, Paris EC, Pontes FM et al. J. Mat. Sci. 2003;38:1175-1183.
25. Marssi ME, Marrec FL, Lukyanchuk IA et al. J. Appl. Phys. 2003;94:3307-3316.
26. Gattu S, Dasari KS, Kocharlakota VR. World Journal of Condensed Matter Physics. 2015;5:346-352.
27. Jameel MH, Hamzah MQ, Arif M, Agam B. Synthesis and characterizations of co-doped TiO_2 nanoparticles via co-precipitation method; 2020.
28. Arif M, Agam B, Jameel MH, Hamzah MQ. Co-precipitation method in synthesis and characterization of $BiFeO_3$ doped with various concentrations of mn nanoparticles for electronic device applications; 2020.